Electronic Supplementary Material (ESI) for Physical Chemistry Chemical Physics.

Static ^{1}H dynamic nuclear polarization with the biradical TOTAPOL: a transition between the solid effect and the cross effect

Daphna Shimon, Akiva Feintuch, Daniella Goldfarb and Shimon Vega*

*Department of Chemical Physics, Weizmann Institute of Science, Rehovot, Israel

E-mail: Shimon.Vega@weizmann.ac.il

1 Analysis of the DNP spectra

The DNP spectra for the 20 mM and 5 mM samples were measured as a function of temperature and as a function of MW irradiation time t_{MW}. All the spectra were then analyzed by decomposing them into two, SE-DNP and CE-DNP, lineshapes, varying their relative contributions as a function of temperature and t_{MW}. Before the analysis we modified the basic SE lineshapes by slightly changing their frequency profiles. To demonstrate the need for these modifications we show in Fig. S1 the analysis of the steady state DNP spectra at 6 K and 10 K for the 20 mM and 5 mM samples, respectively, using the non-modified SE spectra. As can clearly be seen, the best fit spectra deviate from the experimental ones at the frequency edges. The modification of the SE spectra (see Fig. 5), which is explained in the text, corrects for these deviations. In Figs. S2-S9 we show high quality fits of many DNP spectra relying on the modified SE spectra $F_{SE}(\omega_{MW})$ and the original basic CE spectra $F_{CE}(\omega_{MW})$.

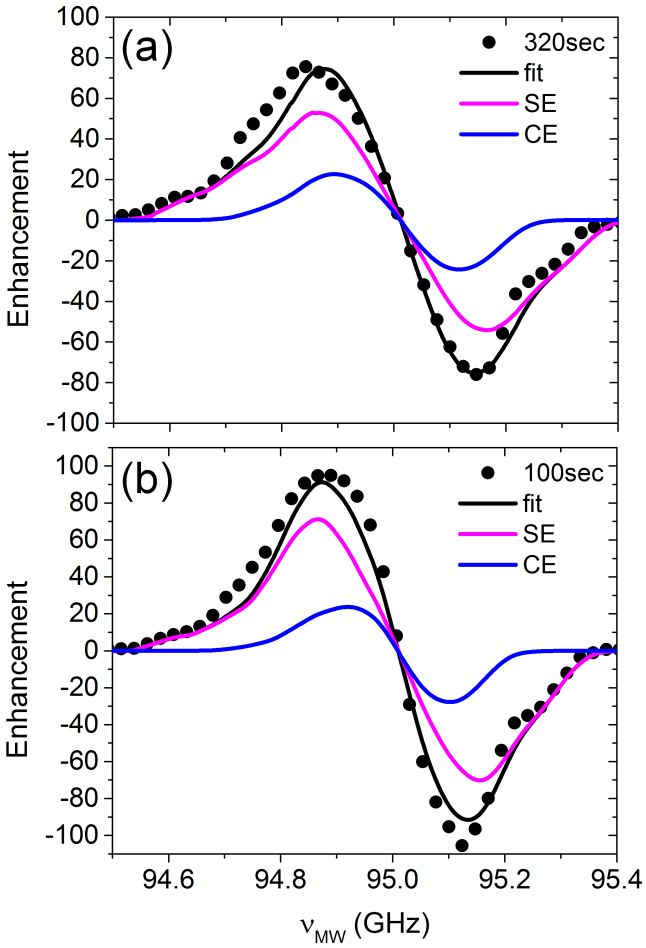

Fig. S1: Analysis of the frequency swept DNP spectra $E(t_{MW}, \omega_{MW})$ (circles) of (a) the 20 mM sample measured at 6 K at t_{MW}=320 sec and of (b) the 5 mM sample measured at 10 K at t_{MW}=320 sec. Shown are the SE contribution $b_{SE}(t_{MW})F^*_{SE}(\omega_{MW})$ (magenta lines), the CE contribution $b_{CE}(t_{MW})F_{CE}(\omega_{MW})$ (blue lines) and the fit $S_{sim}(t_{MW}, \omega_{MW})$ (black lines) done with $F^*_{SE}(\omega_{MW})$ taken exactly as calculated and without modification. The fitting procedure is described in the text.

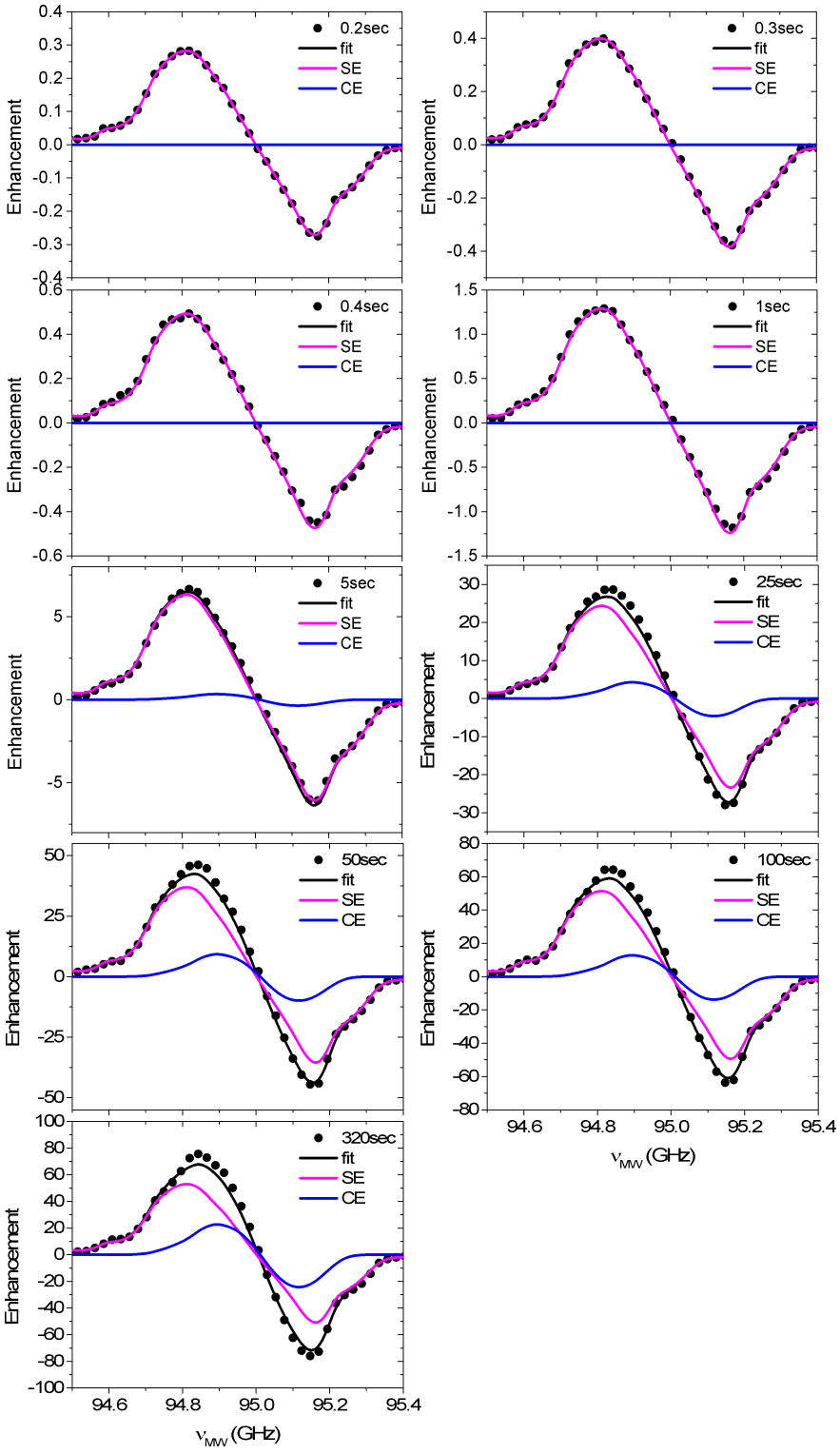

Fig. S2: Analysis of the frequency swept DNP spectra $E(t_{MW}, \omega_{MW})$ (circles) of the 20 mM sample measured at 6 K starting at t_{MW}=0.2 sec and ending with t_{MW} = 320 sec $\approx 5T_{bu}$. Shown are the SE contribution $b_{SE}(t_{MW})F_{SE}(\omega_{MW})$ (magenta lines), the CE contribution $b_{CE}(t_{MW})F_{CE}(\omega_{MW})$ (blue lines) and the fit $S_{sim}(t_{MW}, \omega_{MW})$ (black lines). The fitting procedure is described in the text.

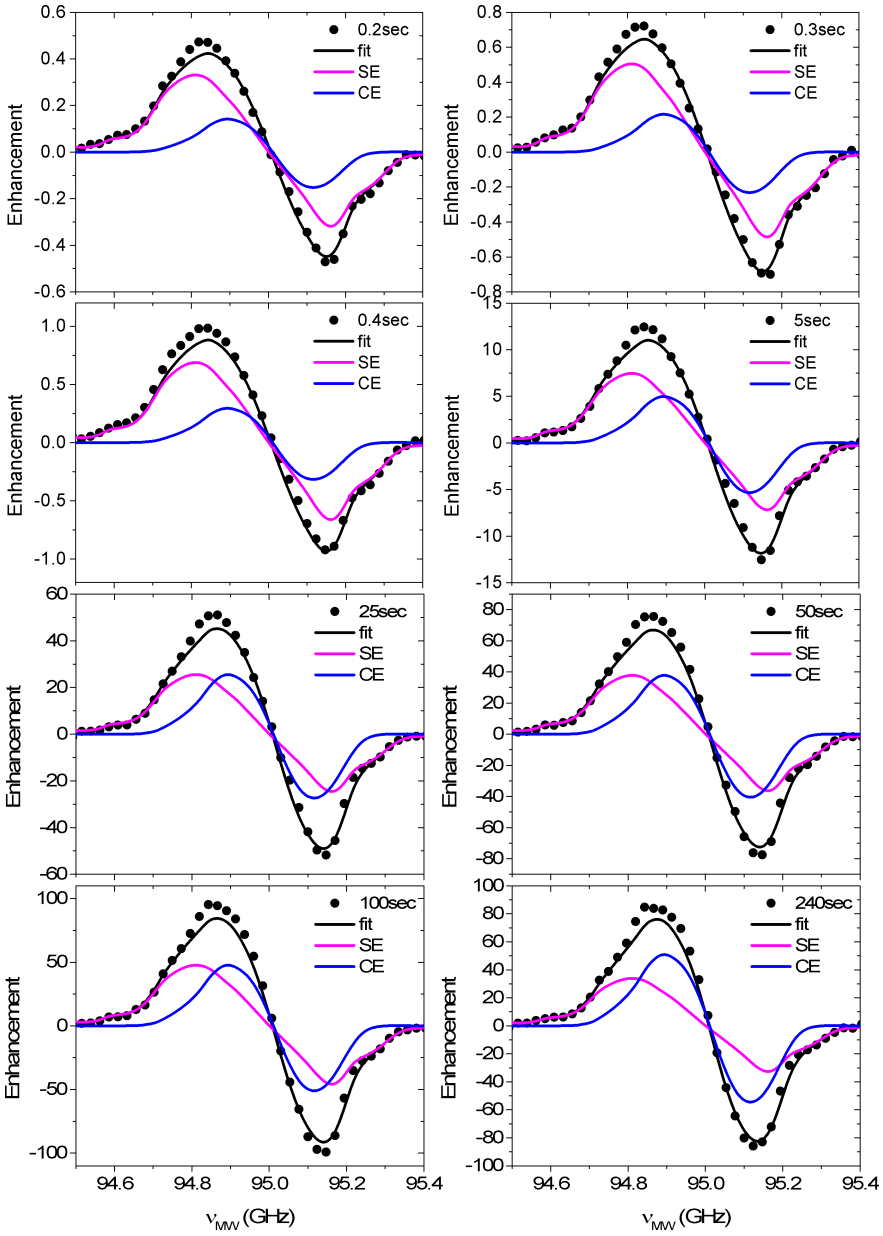

Fig. S3: Analysis of the frequency swept DNP spectra $E(t_{MW}, \omega_{MW})$ (circles) of the 20 mM sample measured at 10 K starting at t_{MW}=0.2 sec and ending with t_{MW} = 240 sec $\approx 5T_{bu}$. Shown are the SE contribution $b_{SE}(t_{MW})F_{SE}(\omega_{MW})$ (magenta lines), the CE contribution $b_{CE}(t_{MW})F_{CE}(\omega_{MW})$ (blue lines) and the fit $S_{sim}(t_{MW}, \omega_{MW})$ (black lines). The fitting procedure is described in the text.

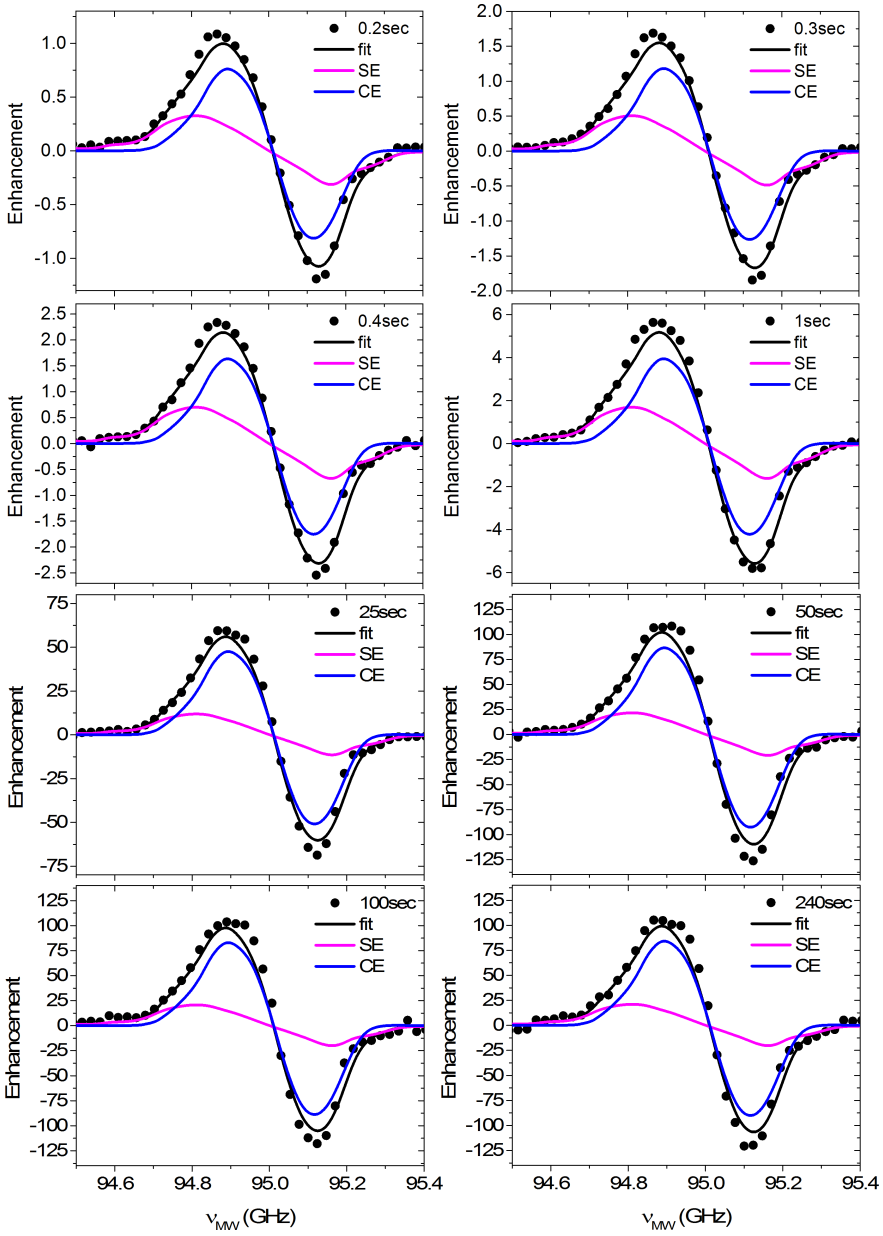

Fig. S4: Analysis of the frequency swept DNP spectra $E(t_{MW}, \omega_{MW})$ (circles) of the 20 mM sample measured at 20 K starting at t_{MW}=0.2 sec and ending with $t_{MW} = 240$ sec $\approx 5T_{bu}$. Shown are the SE contribution $b_{SE}(t_{MW})F_{SE}(\omega_{MW})$ (magenta lines), the CE contribution $b_{CE}(t_{MW})F_{CE}(\omega_{MW})$ (blue lines) and the fit $S_{sim}(t_{MW}, \omega_{MW})$ (black lines). The fitting procedure is described in the text.

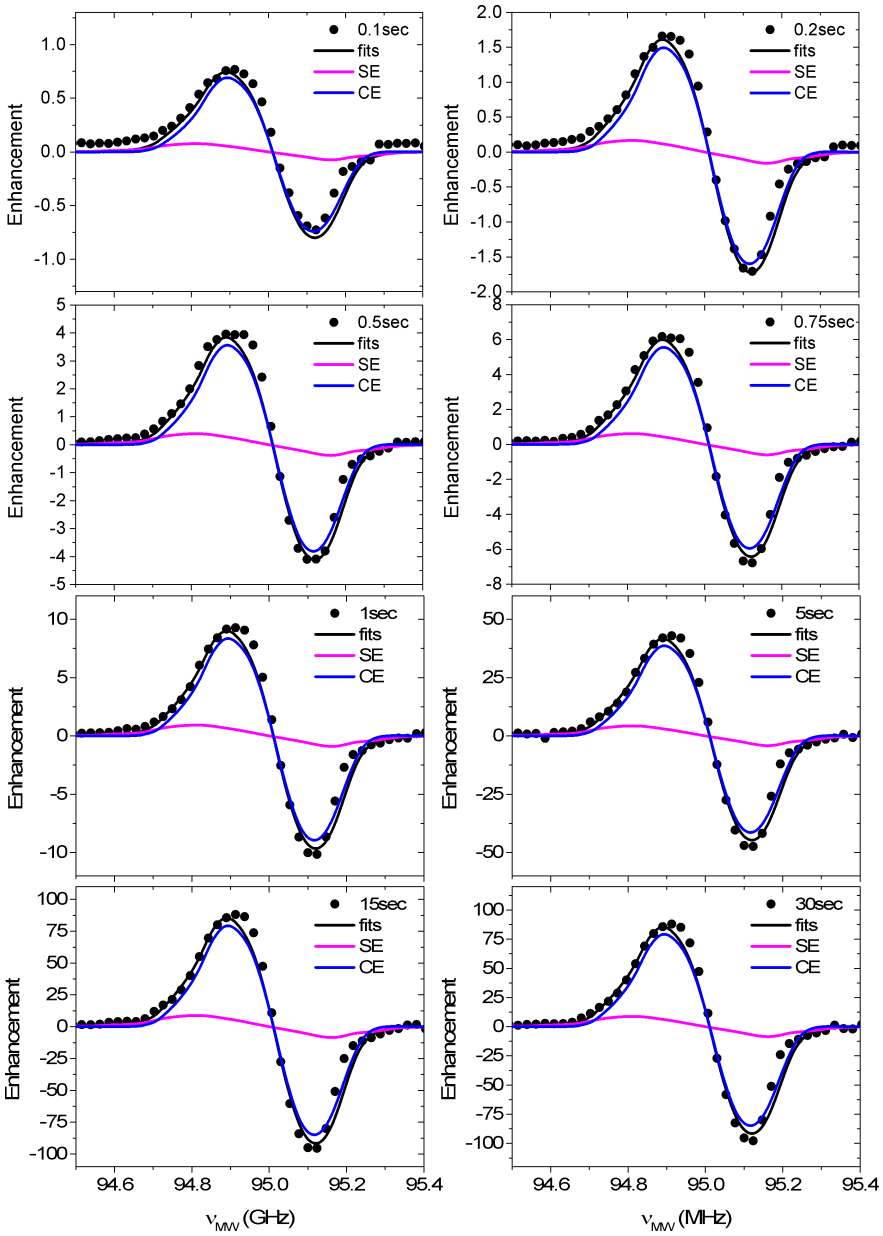

Fig. S5: Analysis of the frequency swept DNP spectra $E(t_{MW}, \omega_{MW})$ (circles) of the 20 mM sample measured at 40 K starting at t_{MW}=0.1 sec and ending with t_{MW} = 30 sec $\approx 5T_{bu}$. Shown are the SE contribution $b_{SE}(t_{MW})F_{SE}(\omega_{MW})$ (magenta lines), the CE contribution $b_{CE}(t_{MW})F_{CE}(\omega_{MW})$ (blue lines) and the fit $S_{sim}(t_{MW}, \omega_{MW})$ (black lines). The fitting procedure is described in the text.

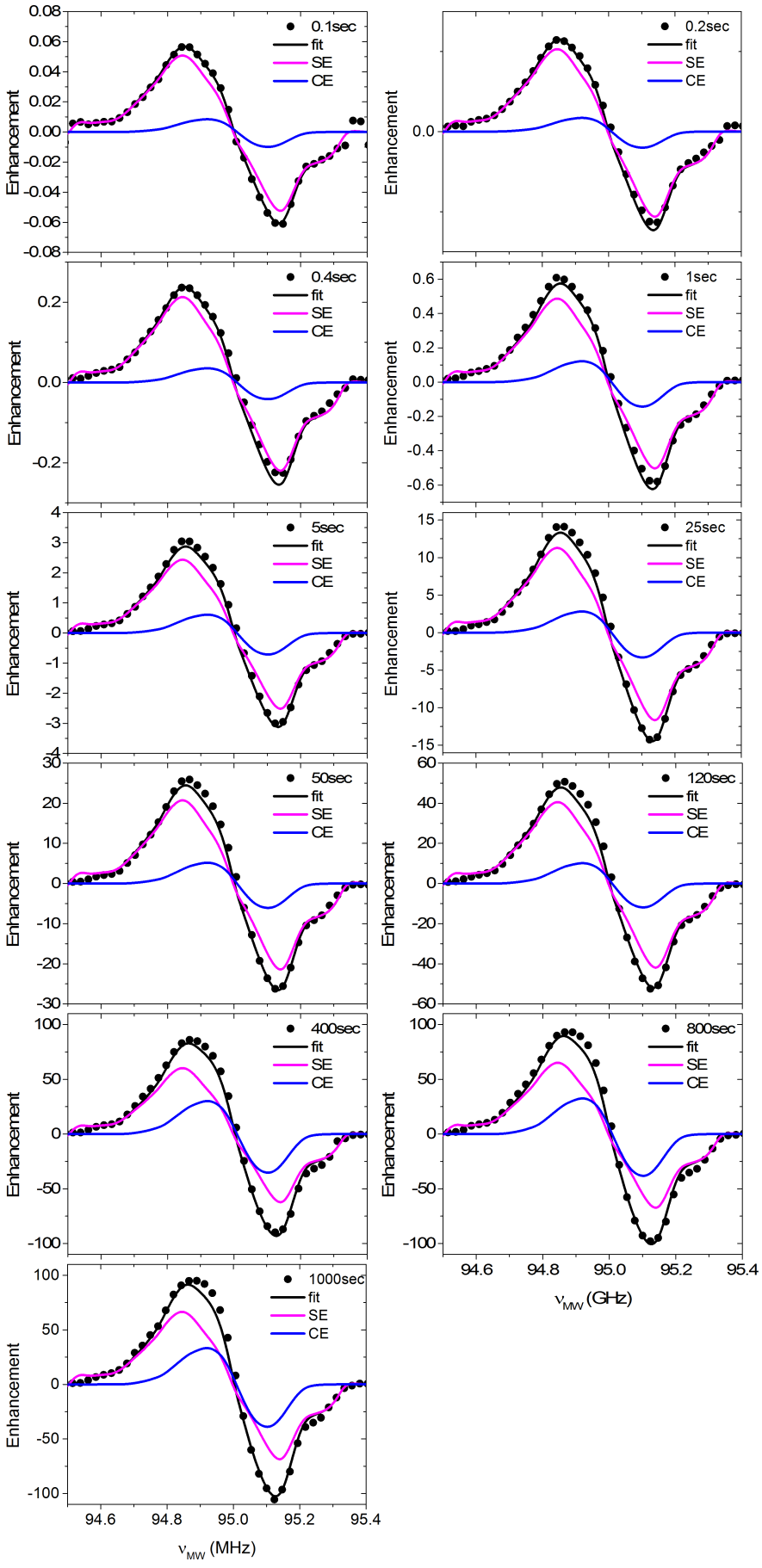

Fig. S6: Analysis of the frequency swept DNP spectra (circles) of the 5 mM sample measured at 10 K starting at t_{MW}=0.1 sec and ending with $t_{MW} = 1000$ sec $\approx 5T_{bu}$. Shown are the SE contribution $b_{SE}(t_{MW})F_{SE}(\omega_{MW})$ (magenta lines), the CE contribution $b_{CE}(t_{MW})F_{CE}(\omega_{MW})$ (blue lines) and the fit $S_{sim}(t_{MW}, \omega_{MW})$ (black lines). The fitting procedure is described in the text.

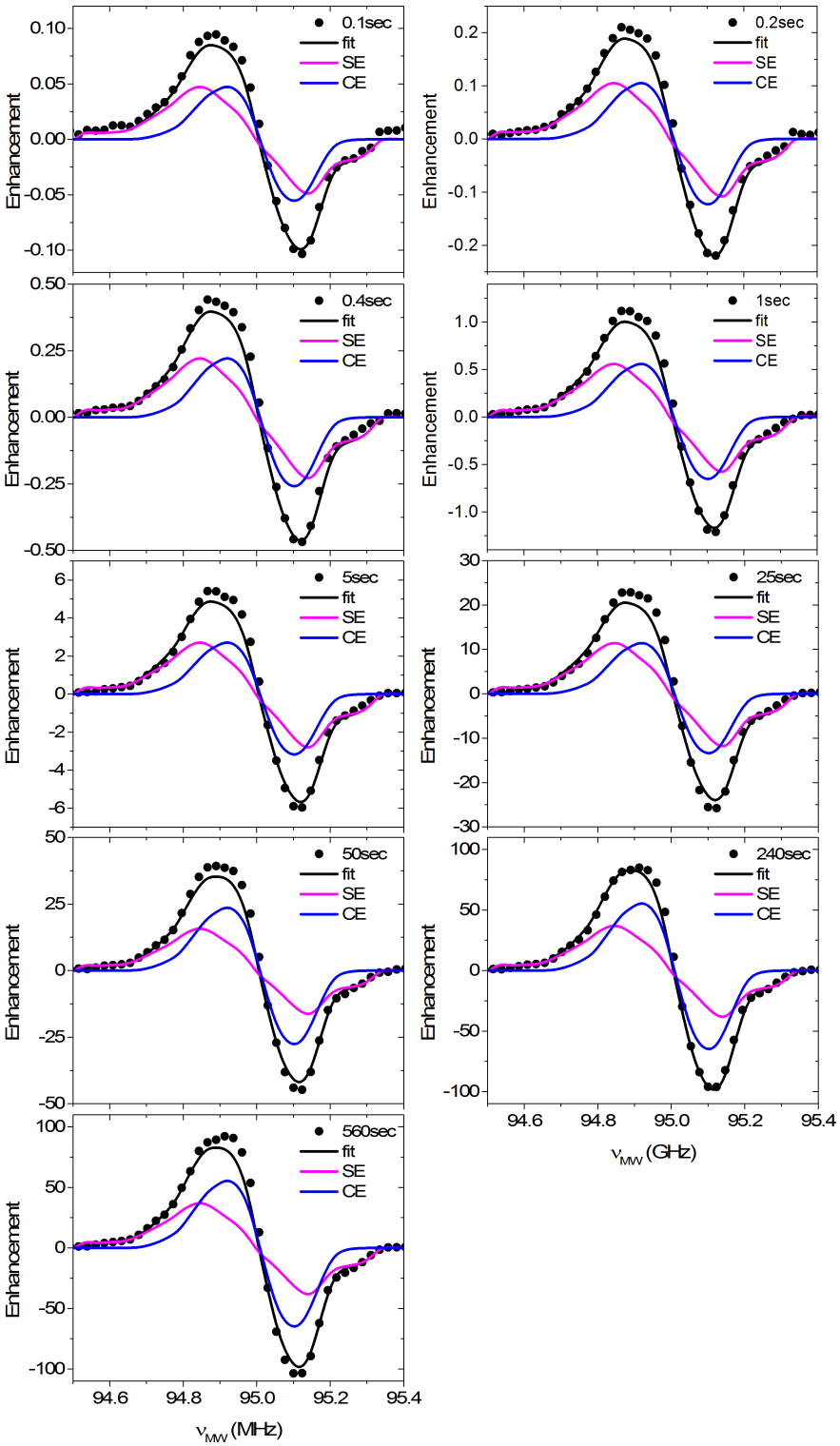

Fig. S7: Analysis of the frequency swept DNP spectra $E(t_{MW}, \omega_{MW})$ (circles) of the 5 mM sample measured at 20 K starting at t_{MW}=0.1 sec and ending with $t_{MW} = 560$ sec $\approx 5T_{bu}$. Shown are the SE contribution $b_{SE}(t_{MW})F_{SE}(\omega_{MW})$ (magenta lines), the CE contribution $b_{CE}(t_{MW})F_{CE}(\omega_{MW})$ (blue lines) and the fit $S_{sim}(t_{MW}, \omega_{MW})$ (black lines). The fitting procedure is described in the text.

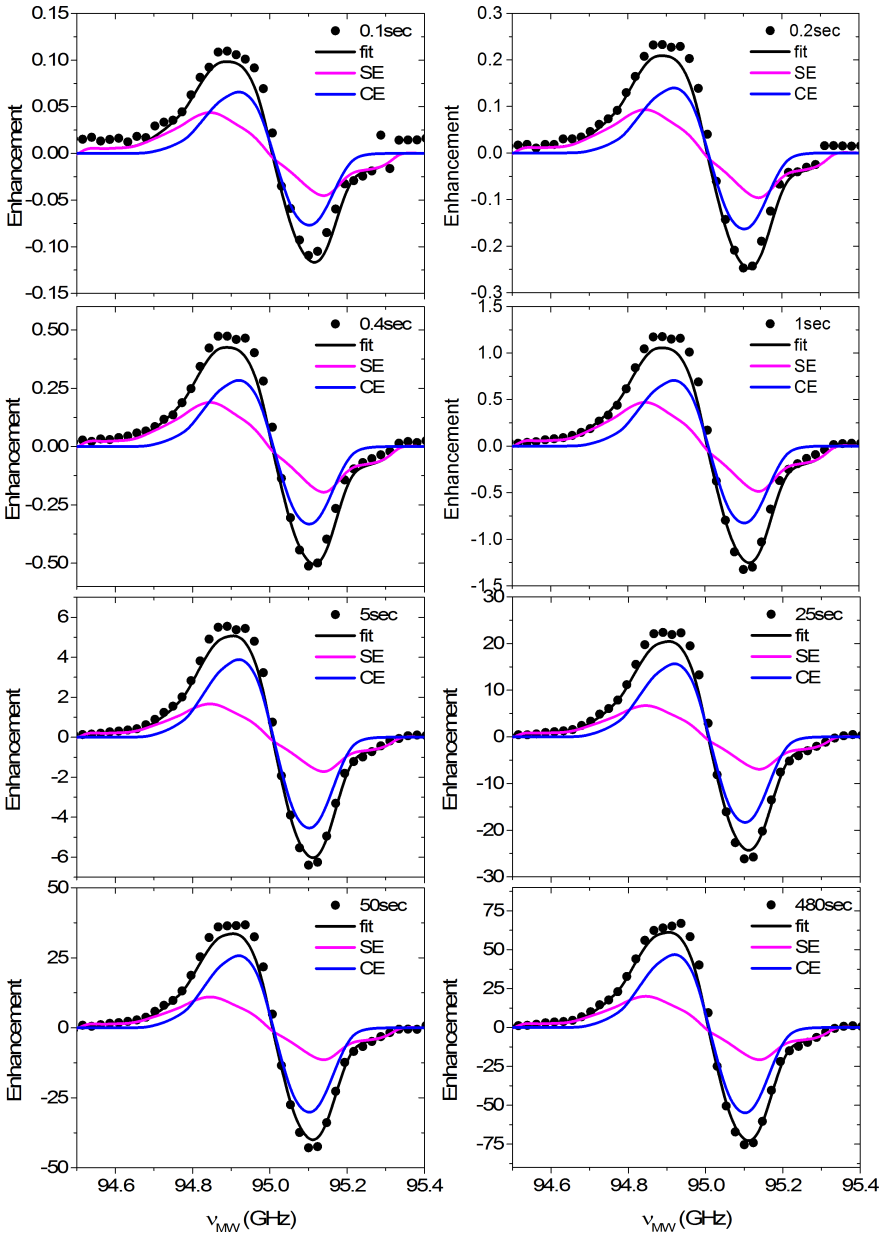

Fig. S8: Analysis of the frequency swept DNP spectra $E(t_{MW}, \omega_{MW})$ (circles) of the 5 mM sample measured at 30 K starting at t_{MW}=0.1 sec and ending with t_{MW} = 480 sec $\approx 5T_{bu}$. Shown are the SE contribution $b_{SE}(t_{MW})F_{SE}(\omega_{MW})$ (magenta lines), the CE contribution $b_{CE}(t_{MW})F_{CE}(\omega_{MW})$ (blue lines) and the fit $S_{sim}(t_{MW}, \omega_{MW})$ (black lines). The fitting procedure is described in the text.

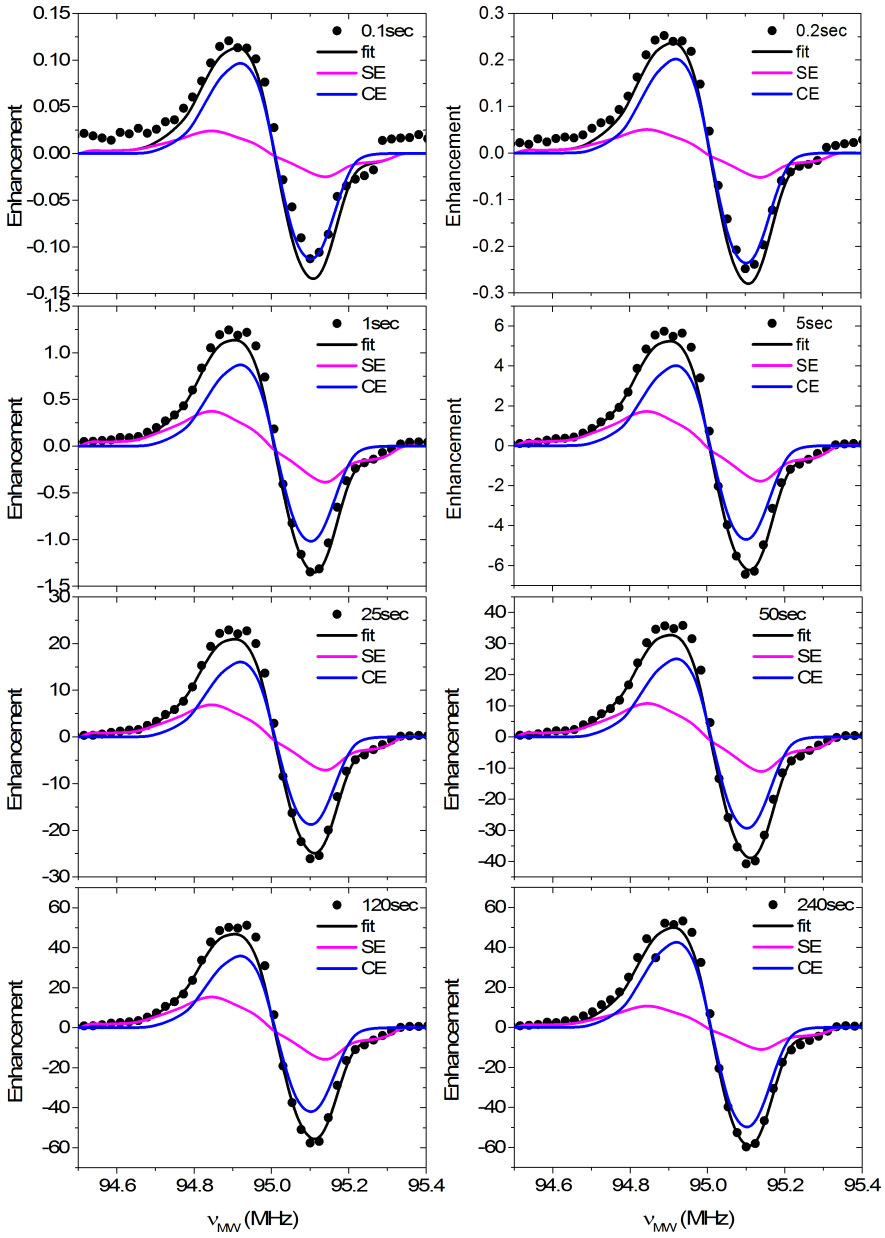

Fig. S9: Analysis of the frequency swept DNP spectra $E(t_{MW}, \omega_{MW})$ (circles) of the 5 mM sample measured at 40 K starting at t_{MW}=0.1 sec and ending with t_{MW} = 240 sec $\approx 5T_{bu}$. Shown are the SE contribution $b_{SE}(t_{MW})F_{SE}(\omega_{MW})$ (magenta lines), the CE contribution $b_{CE}(t_{MW})F_{CE}(\omega_{MW})$ (blue lines) and the fit $S_{sim}(t_{MW}, \omega_{MW})$ (black lines). The fitting procedure is described in the text.

2 TEMPOL DNP spectra

In our previous work on samples of TEMPOL we measured DNP spectra as a function of temperature only after reaching the steady state enhancement and did not measure DNP spectra as a function of t_{MW} [1]. We were able to get good fits at all temperatures. For the 40 mM degassed TEMPOL sample the analysis indicated that at 6 K the DNP spectrum was mainly determined by the SE-lineshape. For comparison with the TOTAPOL results described in this paper, we measured two new DNP spectra of TEMPOL at 6 K; one at $t_{MW} = 0.2$ sec and one at the steady state with $t_{MW} = 240$ sec. Both spectra show very similar shapes and both can be analyzed by the basic non-modified SE and CE shapes as previously described [1]. From these spectra we therefore conclude that for TEMPOL at 6 K and above there is no need to modify the basic SE lineshape.

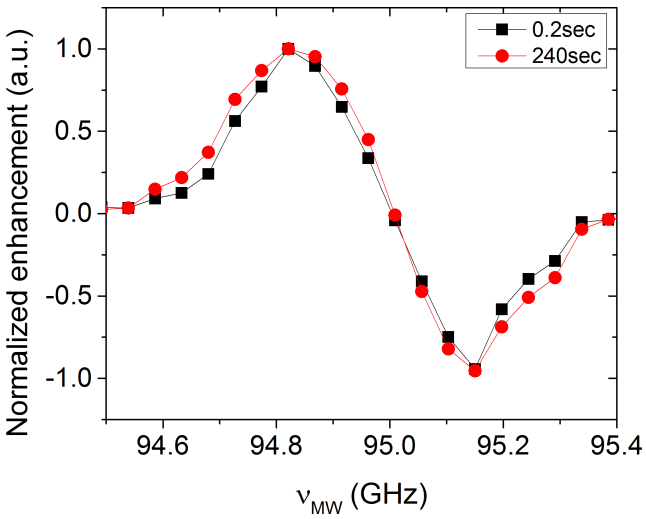

Fig. S10: Normalized frequency swept DNP spectra $E(t_{MW}, \omega_{MW})$ of a 40 mM degassed TEMPOL sample (in 54/46 v% DMSO/H_2O) at $t_{MW} = 0.2$ sec (black squares) and $t_{MW} = 240$sec (red circles). The lines in this figure are to guide the eye.

3 From small to large spin systems

Quantum mechanical based DNP simulations of the spin dynamics of electrons and nuclei are limited by the size of the matrix representing the spin Hamiltonian. For full Liouville space calculations including relaxation our calculations are restricted to 5-6 spins. Clearly more spins are needed in order to describe the macroscopic effects of DNP such as those we see in experiments. In order to study the propagation of nuclear polarization in model systems Hovav et al. [2] used rate equations for the density matrix populations for the SE-DNP mechanism, which allowed simulations of up to 10 spins. Also for the case of SE-DNP, Kockenberger et al. increased the spin system to 25 spins [3]. A more simplified approach to large spin systems is to write rate equations for the dynamics of the polarization of each electron and nuclear spin in the system. The problem with this type of approach is that one is presumably losing the quantum character of the system. In this paper we are interested in understanding the DNP dynamics in real samples. We therefore decided it was essential to use the spin polarization rate equation approach so that we can come as close as possible to simulating real systems. However in order to preserve the quantum nature of the problem, we performed full quantum simulations on small systems to estimate the DNP buildup rate of each nuclear spin. We then assume that these rates are good representatives of the build up rates in large spin systems. For the SE-DNP case the estimation for these rates from small systems is straightforward as we will describe in the next section.

The CE-DNP case is, however, more complex because the effective MW irradiation strength depends not only on the interaction between the electron and nuclear spin but also on the proximity of the electron-nuclear system to the CE-condition [4]. When dealing with a macroscopic sample with many electrons and nuclei the state mixings defining the CE-conditions are complex and it will be necessary to extend the definition of the CE-conditions before we can incorporate those in DNP calculations of larger model system. Therefore at the moment our calculations are restricted to SE-DNP on systems with one electron and many nuclear spins.

After approximating the buildup rates of the nuclei we add spin diffusion terms to the polarization rate equations which spread the nuclear polarization throughout the bulk [5, 6, 7, 8, 9]. Similar rate equations for the polarizations have been used recently by Griffin and coworkers in order to describe the effect of the spin diffusion process on the nuclei close to the electron and the bulk nuclei [10]. Here we use a similar set of coupled rate equations in order to provide a qualitative description of the effects of the change of temperature (and thus of relaxation times) on the SE-DNP enhancement mechanism. As discussed below, the individual MW irradiation rates in our equations are adapted from the quantum mechanical behavior [2, 11] by calculating them from the pseudo-hyperfine interactions and the nuclear Zeeman frequency and neglecting off resonance effects. In

addition a spin diffusion rate is introduced as well as spin-lattice relaxation parameters.

4 A two-dimensional model system of nuclei surrounding an electron

To demonstrate the SE-DNP spin dynamics we composed a two-dimensional square grid of nuclei i surrounding a single electron with a lattice parameter of 3.1 Å (the average distance between protons in bulk water). The purpose of the simulations is to calculate the dependence of the electron and nuclear polarizations, P_e and P_i respectively, on the MW irradiation time t_{MW}. To do so we assign to each nucleus an effective DQ irradiation field (in practice applied at $\omega_e - \omega_n$) of strength

$$\omega_{1,eff,i}^{SE} = 2\pi \frac{|A^{\pm}|}{2\omega_n}\omega_1 = 2\pi \frac{\mu_0 \gamma_e \gamma_H \hbar \cdot 3cos(\theta)sin(\theta)}{4\omega_n r_{e-i}^3}\omega_1, \quad (1)$$

which depends on the distance r_{e-i} between the electron and nucleus i , the angle θ between this vector and the magnetic field, the MW irradiation strength ω_1 and the Larmor frequency of the nuclei ω_n [2, 11]. μ_0 is the permeability of free space and γ_e and γ_H are the gyromagnetic ratios of an electron and a proton, respectively. For protons at a distance of 7 Å $\omega_{1,eff,i}^{SE}$ ≈300 kHz for an applied field of $\omega_1/2\pi = 1\,MHz$. Thus these effective fields $\omega_{1,eff,i}^{SE}$ can easily become two orders of magnitude smaller than the actual applied field ω_1 itself.

In real systems the nuclear dipolar interaction modifies $\omega_{1,eff,i}^{SE}$. As was shown for linear systems this interaction mixes the nuclear spin states spreading the DQ MW matrix elements to states that belong to nuclei that are not directly interacting with the electron and causing their polarization enhancement [2]. This dipolar-assisted DNP enhancement process is of course also present in real systems, thus increasing the area of directly polarized nuclei around the electron. The three dimensionality of real systems prevents this area from expanding by much because of the conservation of the norm of the DQ part of the MW irradiation matrix and the confinement of the polarized area due to the action of T_{1n} [2, 11]. Without a theoretical framework that enables exact evaluation of the dipolar-assisted effective MW fields, we can only mimic the effect of the nuclear dipolar interaction by spreading the direct effective field $\omega_{1,eff,i}^{SE}$ of each nucleus i to its neighbors. In the present calculations we distributed each $\omega_{1,eff,i}^{SE}$ value between the nucleus i itself, leaving a field $\omega_{i,i}^{SE} = f_{i,i}\omega_{1,eff,i}^{SE}$, and contributing to its neighboring nuclei j a field $\omega_{j,i}^{SE} = f_{j,i}\omega_{1,eff,i}^{SE}$, with $f_{i,i} = \frac{1}{\sqrt{9}}$ and $f_{j,i} = \frac{2}{4\sqrt{9}}$ for the 4 nearest-neighbor nuclei j that are 3.15 Å away from nucleus i and $f_{j,i} = \frac{2}{8\sqrt{9}}$ for the 8 next-nearest-neighbor nuclei j removed by 6.25 Å or less from nucleus i. After this redistribution

of the effective MW fields the effective excitation rate of each nucleus k is defined as

$$R_{bu,k}^{SE} \equiv (\sum_j \omega_{j,k}^{SE})^2 T_{2x} \tag{2}$$

with the introduction of an electron-nuclear cross relaxation time T_{2x} [2, 11]. The $f_{j,i}$ values are chosen such that $\sum_j (f_{j,i})^2 = 1$ so that

$$\left\{\omega_{1,eff,i}^{SE}\right\}^2 = \sum_j \left\{\omega_{j,i}^{SE}\right\}^2 \tag{3}$$

and the overall effective irradiation rate $\sum_i R_{bu,i}^{SE}$ stays constant in the system. In this way the nuclear dipolar interaction does not modify the overall buildup rate of the system, but changes the individual rates of the different nuclei.

The electron spin lattice relaxation rate R_{1e} is chosen to be much larger than all $R_{bu,i}^{SE}$, such that it has little effect on the buildup times of the nuclei. As long as R_{1e} is large the electron states are maintained at their Boltzmann distribution and the MW field determines the buildup of nuclear polarization. For small R_{1e} values (approaching the nuclear spin-lattice relaxation rate) the electron polarization cannot recover from the partial saturation of the DQ or ZQ transition and as a result it lowers the nuclear polarization [11].

The nuclear spin-lattice relaxation rates $R_{1,i}$ of nucleus i can have one of two values: when i belongs to the "core nuclei" that are at a distance of 9 Å or less from the electron $R_{1,i} = R_{1c}$ [11] and for the rest of the nuclei $R_{1,i} = R_{1n}$. To represent the fact that the core nuclei relax faster than the bulk nuclei due to hyperfine relaxation we chose $R_{1c} = 10 \cdot R_{1n}$.

The spin diffusion is represented in the polarization rate equations by a dipolar relaxation rate $R_{1d,ij}$, defining the characteristic time of equalization of the polarization of neighboring nuclei, as was done in earlier studies [7, 8, 12, 13]. The quenching of the nuclear dipolar interaction by the electron-nuclear hyperfine interaction is taken into account by using a spin diffusion rate $R_{1d,ij}$ between core nuclei i and j that is 100 times smaller than $R_{1d,ij}$ between bulk nuclei i and j. In all cases $R_{1d,ij} \gg R_{1,i}$ such that all bulk nuclei are polarized almost uniformly and all nuclei (except for part of the core nuclei) experience about the same polarization buildup rate R_{bu}^{SE} and reach about the same end polarization P_{end}^{SE}.

The differential equations for the electron and nuclear polarization, $P_e = P_e(t_{MW})$ and $P_i = P_i(t_{MW})$, used during our simulations are:

$$\frac{dP_i}{dt_{MW}} = -R_{1,i}P_i - \sum_{(j)_i} \frac{1}{2} R_{1d,ij}(P_i - P_j) + \frac{1}{2} R_{bu,i}(P_i - P_e) \tag{4}$$

$$\frac{dP_e}{dt_{MW}} = -R_{1e}(P_e - P_{e0}) + \sum_i \frac{1}{2} R_{bu,i}(P_i - P_e) \tag{5}$$

where the sum over $(j)_i$ is restricted to nuclei that are nearest neighbors of i, and where the number of nuclei in the model are N_n. The initial electron polarization equals $P_{e0} = P_e(0)$ and in all simulations we neglected the initial nuclear Boltzmann polarizations. We also ignore off-resonance effects due to frequency shifts due to hyperfine and dipolar interactions and off-resonance irradiation on the electron SQ transitions. Solving this set of equations results in the time dependent nuclear polarizations and their steady state values $P^{SE}_{end,i}$.

The effect of fast spin diffusion and the dependence of the SE steady state polarizations on R_{1n} is shown in Figs. 10-11 of the main text. Fig. 10a shows the distance and angular dependence of the nuclear polarization without spin diffusion ($R_{1d} = 0\ sec^{-1}$). The angular dependence caused by the pseudo-secular hyperfine interaction is partially wiped out by the dipolar-assisted DNP mechanism. Figs 10b-c show the same model system with spin diffusion, where lengthening R_{1n} increases $P^{SE}_{end,i}$. Fig. 11 summarizes the values of $P^{SE}_{end} = 1/N^{SE}_n \sum_i P^{SE}_{end,i}$ and $R^{SE}_{bu} = 1/N^{SE}_n \sum_i R^{SE}_{bu,i}$ as a function of R_{1n} and the number of nuclei N^{SE}_n in the grid. These figures are described in more detail in the main text. As the buildup times are proportional to T_{2x}, increasing its value increases the individual buildup rates $R^{SE}_{bu,i}$, extends the area of direct polarization around the electron and increases both P^{SE}_{end} and R^{SE}_{bu}.

In real samples most nuclei are polarized by more than one SE-active electron. When irradiating with a certain frequency ω_{MW} electrons with a Larmor frequency of $\omega_{MW} + \omega_n$ result in positive nuclear polarization (DQ irradiation) and electrons at $\omega_{MW} - \omega_n$ result in negative nuclear polarization (ZQ irradiation). Our DNP spectrum analysis model assumes that the final enhancement when irradiating at ω_{MW} is proportional to the difference between the number of electrons at $\omega_{MW} + \omega_n$ and the number of electrons at $\omega_{MW} - \omega_n$. The effect of different electrons partially canceling each other's DNP induced polarization is shown in Fig. S1. Here the electron in the bottom right corner results in positive polarization and the electron in the top right corner results in negative polarization. The hyperfine interactions of the negative polarizing electron with the nuclei were artificially weakened by 80% in order to show the averaging of the nuclear polarization originating from two electron polarizing sources. This simulation was performed by extending the rate equations described above to include a second electron spin.

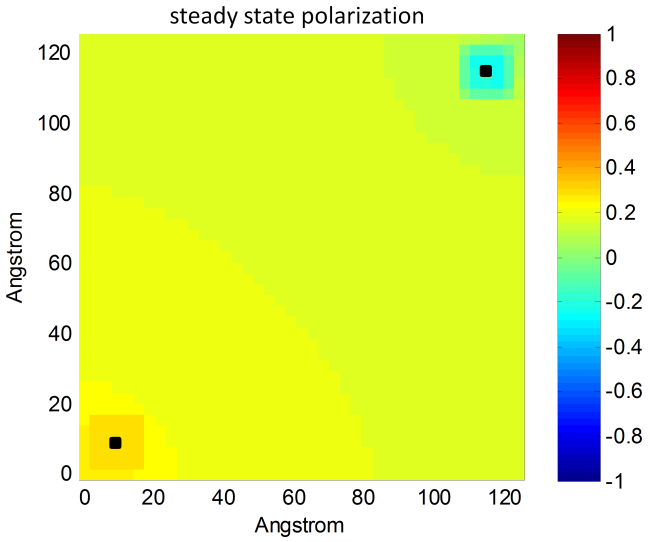

Fig. S11: 2D contour plot of the steady state nuclear polarization for a system of two SE electrons (marked by black pixels), one in the lower left corner with MW irradiation on its DQ transition and one in the upper right corner with MW irradiation on its ZQ transition. The hyperfine interactions of the negative polarizing electron with the nuclei were artificially weakened by a 80%. Each nucleus is a pixel whose color represents the nuclear polarization normalized to the electron thermal equilibrium polarization. The nuclei are 3.1 Å apart in both dimensions, and there are 960 nuclei in all. The other parameters of the system are: $R_{1e} = 100\ sec^{-1}$, $R_{1c} = 10 \cdot R_{1n}\ sec^{-1}$, $R_{1n} = 10^{-2}\ sec^{-1}$, $R^b_{1d} = 10^3\ sec^{-1}$, $R^c_{1d} = 10\ sec^{-1}$, $\omega_1 = 1$ MHz and $T_{2x} = 5\mu sec$. The rate equations used to calculate these plots are given above.

References

[1] D. Shimon, Y. Hovav, A. Feintuch, D. Goldfarb and S. Vega, Phys. Chem. Chem. Phys., 2012, 14, 5729-5743.

[2] Y. Hovav, A. Feintuch and S. Vega, J. Chem. Phys., 2011, 134, 074509.

[3] A. Karabanov, d. D. van, L. J. Edwards, I. Kuprov and W. Kockenberger, Phys. Chem. Chem. Phys., 2012, 14, 2658-2668.

[4] Y. Hovav, A. Feintuch and S. Vega, Journal of Magnetic Resonance, 2012, 214, 29-41.

[5] A. Abragam and M. Goldman, Reports on Progress in Physics, 1978, 41, 395.

[6] O. S. Leifson and C. D. Jeffries, Phys. Rev., 1961, 122, 1781.

[7] M. Afeworki and J. Schaefer, Macromolecules, 1992, 25, 4092-4096.

[8] S. F. J. Cox, S. F. J. Read and W. Th. Wenchebach, Journal of Physics C: Solid State Physics, 1977, 10, 2917.

[9] M. Ernst and B. H. Meier, Studies in Physical and Theoretical Chemistry, 84, (Elsevier, 1998) .

[10] A. A. Smith, B. Corzilius, A. B. Barnes, T. Maly and R. G. Griffin, J. Chem. Phys., 2012, 136.

[11] Y. Hovav, A. Feintuch and S. Vega, J. Chem. Phys., 2011, 134, 074509.

[12] A. E. Dementyev, D. G. Cory and C. Ramanathan, Phys. Rev. B, 2008, 77, 024413.

[13] A. Abragam, Principles of Nuclear Magnetism (Clarendon Press, Oxford, 1961).